Supporting Information

Mitigating the amorphization of perovskite layers by using atomic layer deposition of alumina

*Mayank Kedia[ab], Chittaranjan Das[*ab], Malgorzata Kot[c,k], Yenal Yalcinkaya[d], Weiwei Zuo[b], Kenedy Tabah Tanko[e], Peter Matvija[f], Mikel Ezquer[g], Iñaki Cornago[g], Wolfram Hempel[h], Florian Kauffmann[i], Paul Plate[j], Monica Lira-Cantu[e], Stefan A.L. Weber[ad], Michael Saliba[*ab]*

[a]Institute for Photovoltaics (*ipv*), Research Center SCoPE, and Integrated Quantum Science and Technology Center (IQST), University of Stuttgart, Pfaffenwaldring 47, 70569 Stuttgart, Germany

[b]Helmholtz Young Investigator Group, IMD-3 Photovoltaik, Forschungszentrum Jülich, 52425 Jülich, Germany

[c]Chair of Applied Physics and Semiconductor Spectroscopy, Brandenburg University of Technology Cottbus-Senftenberg, Konrad-Zuse-Straße 1, 03046 Cottbus, Germany

[d]Max Planck Institute for Polymer Research, Ackermannweg 10, 55128 Mainz, Germany

[e]Catalan Institute of Nanoscience and Nanotechnology (ICN2), CSIC and The Barcelona Institute of Science and Technology, 08193 Bellaterra, Barcelona, Spain

[f]Charles University, Faculty of Mathematics and Physics, Department of Surface and Plasma Science, V Holešovičkách 2, Prague, Czech Republic

[g]National Renewable Energy Centre of Spain (CENER), Ciudad de la Innovación 7, 31621, Sarriguren, Spain

[h]Zentrum für Sonnenenergie und Wasserstoff Forschung Baden-Württemberg (ZSW), 70563 Stuttgart, Germany

[i]SRF Advanced Materials Innovation and Characterization (AMICA), University of Stuttgart, 70569 Stuttgart, Germany

[j]SENTECH Instruments GmbH, Schwarzschildstraße 2, 12489 Berlin, Germany

[k]Present Address: Faculty of Electronics, Photonics and Microsystems, Wroclaw University of Science and Technology, Janiszewskiego 11/17, Wroclaw 50-372, Poland

Corresponding Authors

***Chittaranjan Das** chittaranjan.das@ipv.uni-stuttgart.de

***Michael Saliba** michael.saliba@ipv.uni-stuttgart.de

Keywords

Perovskite, ALD, Al_2O_3, spiro-OMeTAD degradation, amorphization

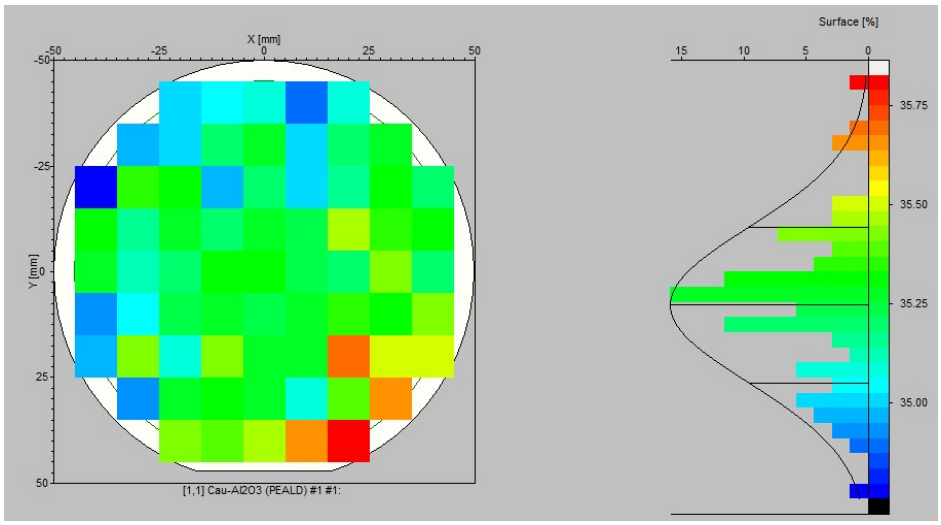

Figure S1. Mapping of thickness distribution after ALD-Al_2O_3 deposition on the Si wafer at 69 points. The average thickness after 600 cycles was 35.24 nm with a standard deviation of <0.2 nm on an area of ~78.54 cm^2. This shows the uniformity of the ALD coating on a large substrate.

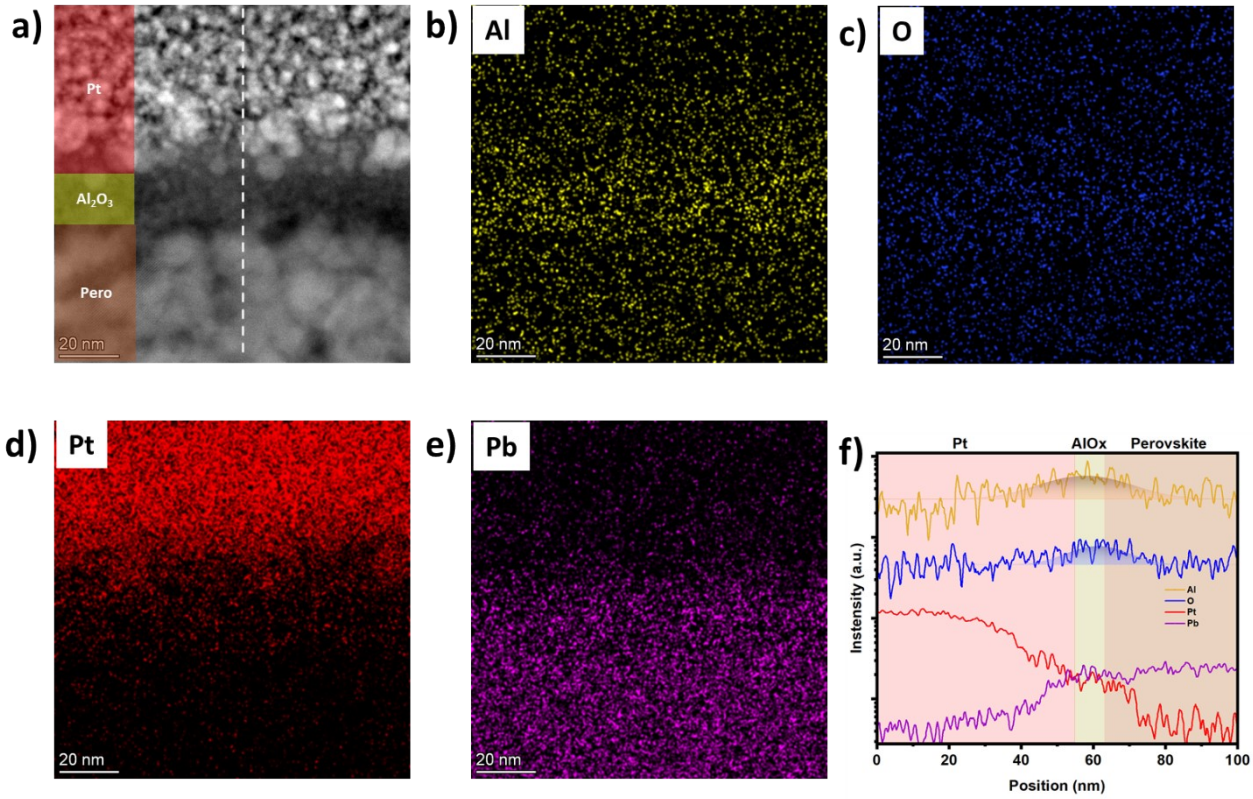

Figure S2. a) TEM image of the cross-section of sputtered Pt and ALD-Al_2O_3 on top of a perovskite with corresponding EDX line scan (in white). b-e) EDX mapping of the elemental distribution of b) Al (yellow), c) O (blue), d) Pt (red), and e) Pb (violet). f) Line distribution of Al, O, Pt, and Pb in the cross-sectional TEM image. The Al and O line spectra were fitted using Gaussian profiles.

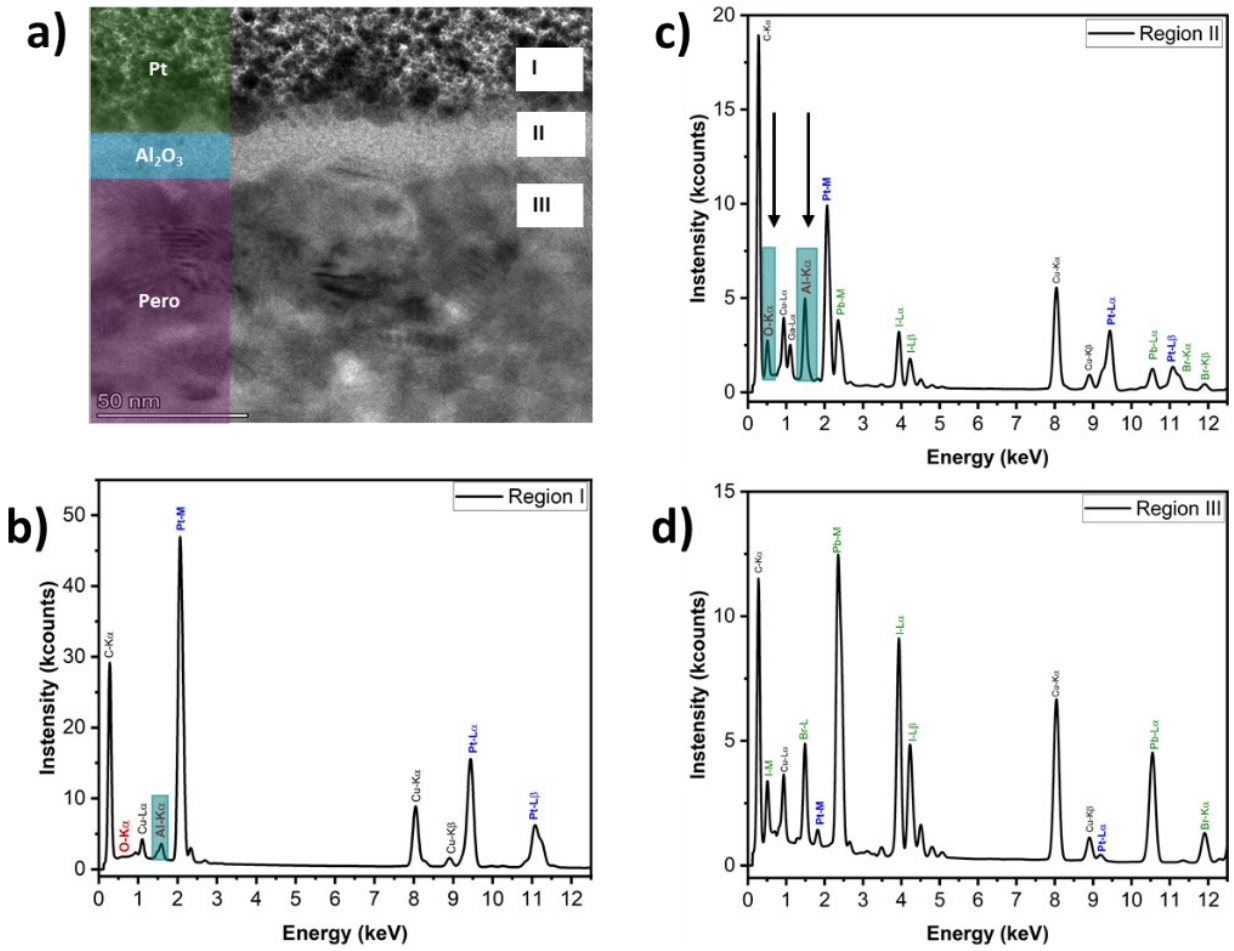

Figure S3. a) TEM image of the cross-section of ALD-Al_2O_3 on top of the perovskite marked with regions I, II, and III for sputtered Pt, ALD-Al_2O_3, and perovskite, respectively. b-d) EDX spectra of regions I, II, and III for sputtered Pt, ALD-Al_2O_3, and the perovskite, respectively. The arrows indicate the position of oxygen and aluminum.

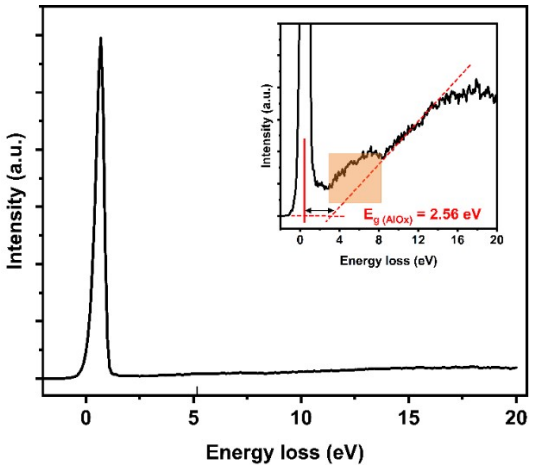

Figure S4. Wide-range reflection electron energy loss (REEL) spectra of ALD-Al_2O_3 formed on a perovskite surface. The primary electron energy was 50 eV. The inset in the figure shows a magnified view of the REEL spectrum to calculate the bandgap by measuring the energy loss at which the inelastic scattering of electrons (slanted dotted red line) begins to occur from the elastic peak (center solid red line).

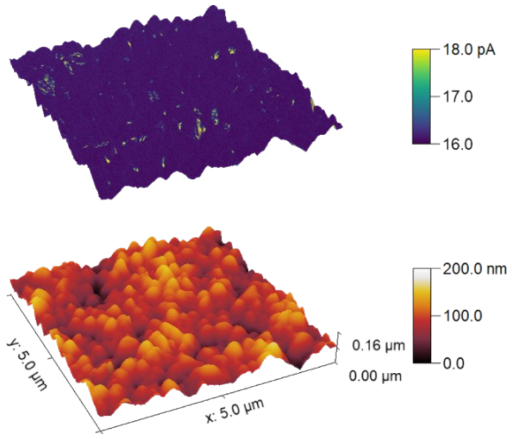

Figure S5. 3D conductive atomic force microscopy (c-AFM) images of the ALD-2 nm films with the current contrast overlaid on the topological image collected over the same area, revealing the microstructure-specific response in the dark at 400 mV. The scale was the same for the uncoated and ALD-2nm films and fixed from 16 pA to 18 pA.

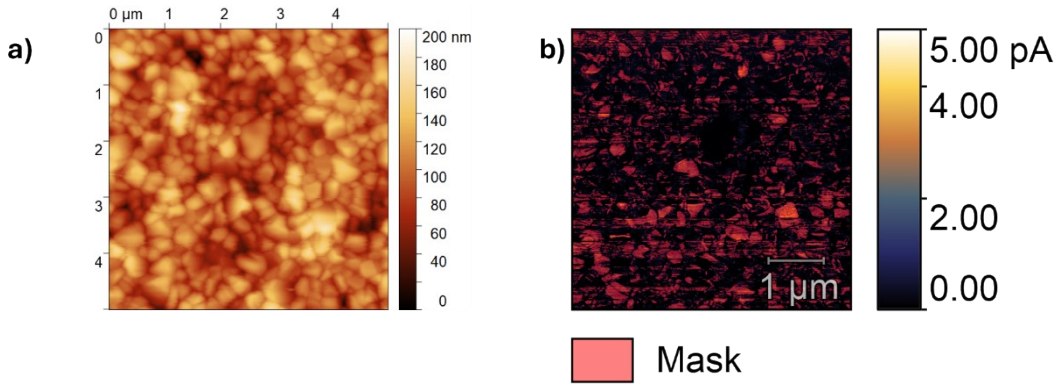

Figure S6. Two-dimensional images of 5 µm × 5 µm region of uncoated perovskite thin film (same magnification): (a) topography, (b) dark I_{SC} with a mask for 0.5 pA.

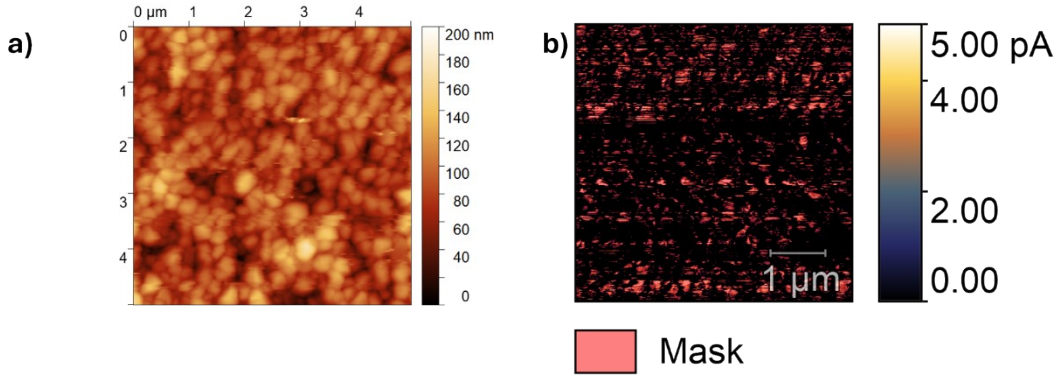

Figure S7. Two-dimensional images of 5 µm × 5 µm region of ALD-0.75nm perovskite thin film (same magnification): (a) topography, (b) dark I_{SC} with a mask for 0.5 pA.

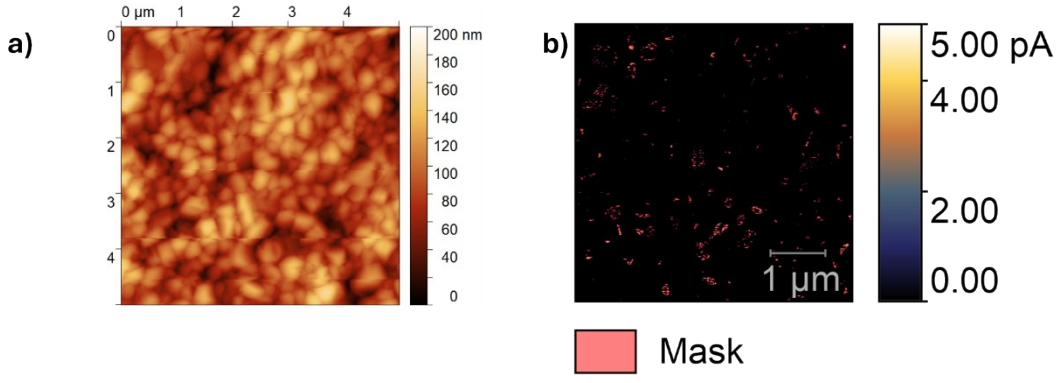

Figure S8. Two-dimensional images of 5 µm × 5 µm region of the ALD-2nm perovskite thin film (same magnification): (a) topography, (b) dark I_{SC} with a mask for 0.5 pA.

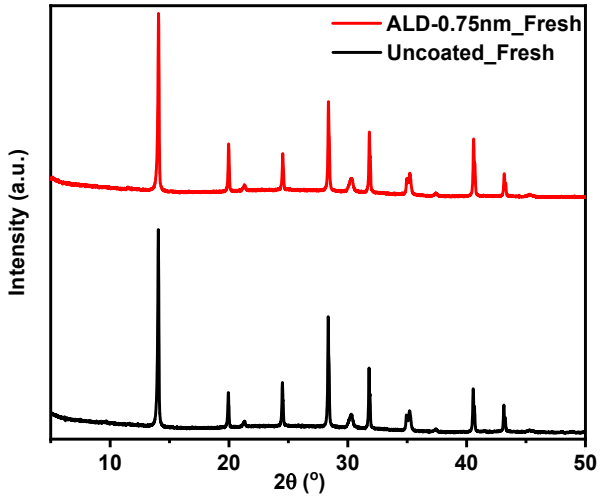

Figure S9. XRD of the fresh uncoated and ALD-0.75nm perovskite films.

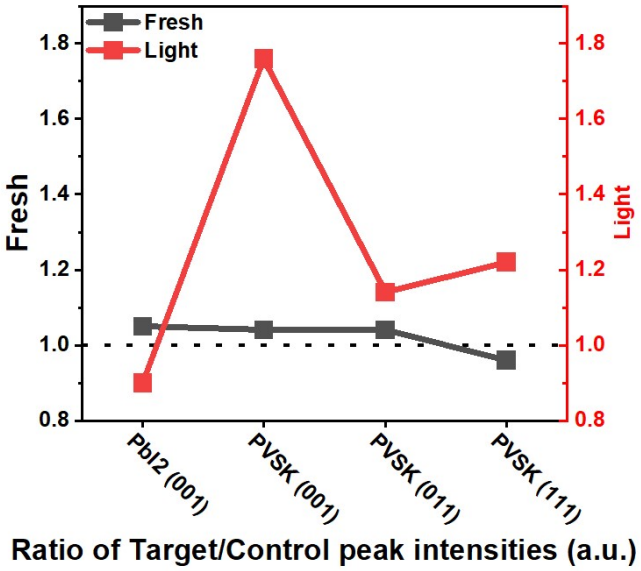

Figure S10. The ratio of the intensity at various reflections of perovskite (PVSK) and PbI_2 for uncoated (Control) and ALD-0.75nm (Target) perovskite films for fresh and aged (light) samples.

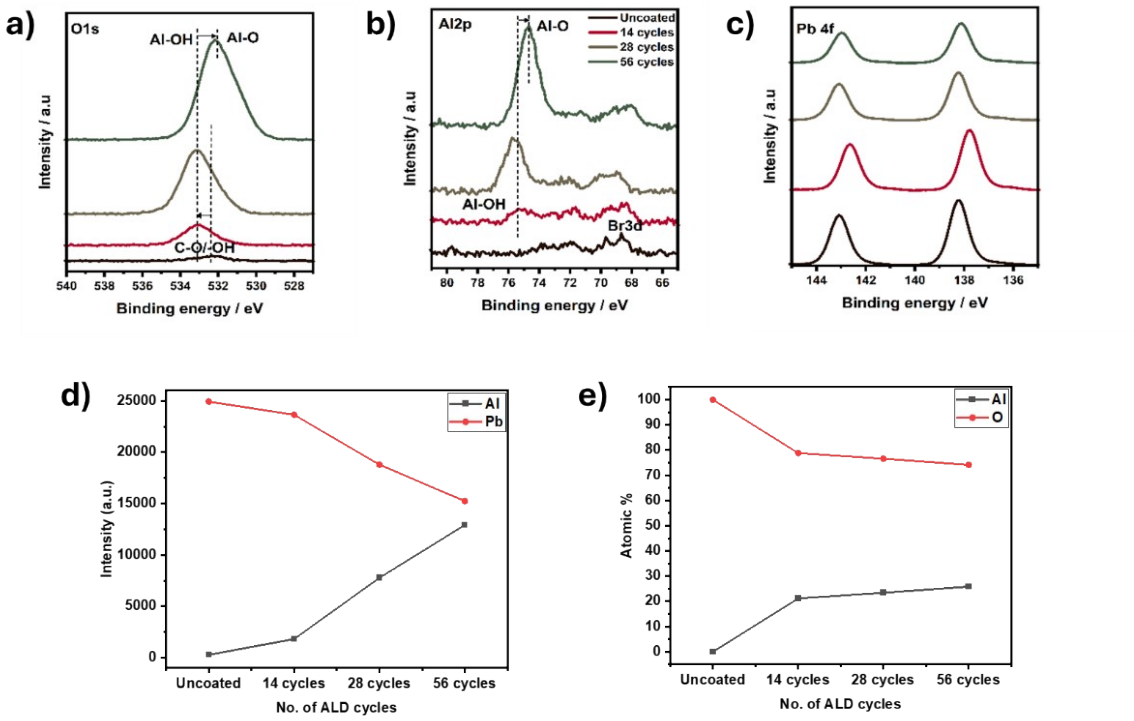

Figure S11. XPS spectra of a) O1s, b) Al2p, and c) Pb4f from the uncoated and various ALD thicknesses on the perovskite films. d) Intensity ratio of Al and Pb e) Atomic concentrations of Al and O after baseline correction of the ALD-AlOx film thickness (as a function of ALD cycles) were obtained from XPS measurements, namely Pb 4f, Al 2p, and O 1s.

Although surface -OH groups are considered the most common chemisorption sites for TMA on Si substrates, earlier reports have shown that TMA can react with methylammonium (MA = $CH_3NH_3^+$) cations from the perovskite (in the absence of -OH groups) on the investigated perovskite to form alumina.[1] Previous work on ALD on MA-rich perovskites also supports this, where SEM images showed degradation after ALD due to voids in the MA-rich areas.[2] Thus, we have performed a series of growth experiments and XPS analysis of the ALD layer with three different thicknesses, 14 cycles (~0.75 nm), 28 cycles (~2 nm), and 56 cycles (~4 nm) on FA-rich perovskite. Hence, we hypothesize the following growth mechanism:

1. The presence of a broad O1s peak, in **Figure S11a**, on the pristine perovskite (without any ALD layer) at binding energies (B.E.) 531.5 – 533.0 eV is characteristic of C-O (organic bond) and O-H (surface hydroxyl) groups at higher and lower B.E., respectively. The presence of surface hydroxyl groups on pristine perovskites could have various origins, such as the presence of oxygen in the glove box or the presence of an unremoved DMSO solvent, as reported in our recent work.[3] We posit that these hydroxyl (–OH) bonds are uniformly present on the surface.

2. The first cycle of TMA could react with the –OH bonds present on the surface and function as the first anchoring site for the next ALD cycle. With the subsequent ALD half-cycle, the chemisorbed Al-OH reacts with H_2O, leading to $Al_2O_x(OH)_{6-2x}$ at room temperature.[4] The peak shift of Al2p (and other core levels of perovskite such as Pb4f) in **Figure S11b** and **Figure S11c** towards lower BE values after initial ALD cycles has been also observed previously and can be

attributed mainly to the presence of OH groups in the film and, in addition, to a filling/de-filling of excitonic states, i.e., charging/recharging processes, resulting in Fermi energy shifts.[5]

3. In the O1s region of **Fig. S11a**, it can be seen that after 14 ALD cycles a shift towards higher B.E. from 532.1 eV to 533.1 eV, as compared to the C-OH bond (marked with a left arrow). Its binding energy value of about 533 eV suggests that the Al is bonded with OH groups. While increasing the number of ALD cycles we observe a higher intensity of the new peak at about 532.1 eV that can be attributed to alumina (marked with a right arrow).

4. With further deposition cycles, we can also see a transition from the Al-OH bond (B.E. of 75.6 eV) dominated to the Al-O bond (B.E. of 74.7 eV), as the final thickness of the ALD layer reaches 4 nm This shows that the first few nanometers of the composition of ALD alumina are not strictly stoichiometric Al_2O_3 but can rather be described as AlOx.

In addition, we have shown the ratio of the peak intensities of Pb4f and Al2p in **Figure S11d**. The intensity of the Pb signal decreased, and the intensity of the Al signal increased substantially. This is in good agreement with the exponential decay in the electron signal coming from the underlying perovskite (Pb-based) due to a uniform coverage of a thin film on the top.[6] Further, we have also shown the atomic percentage ratio of Al and O with increasing ALD cycles in **Figure S11e**. This also indicates a non-stoichiometric ratio of Al and O in the ultrathin ALD film.

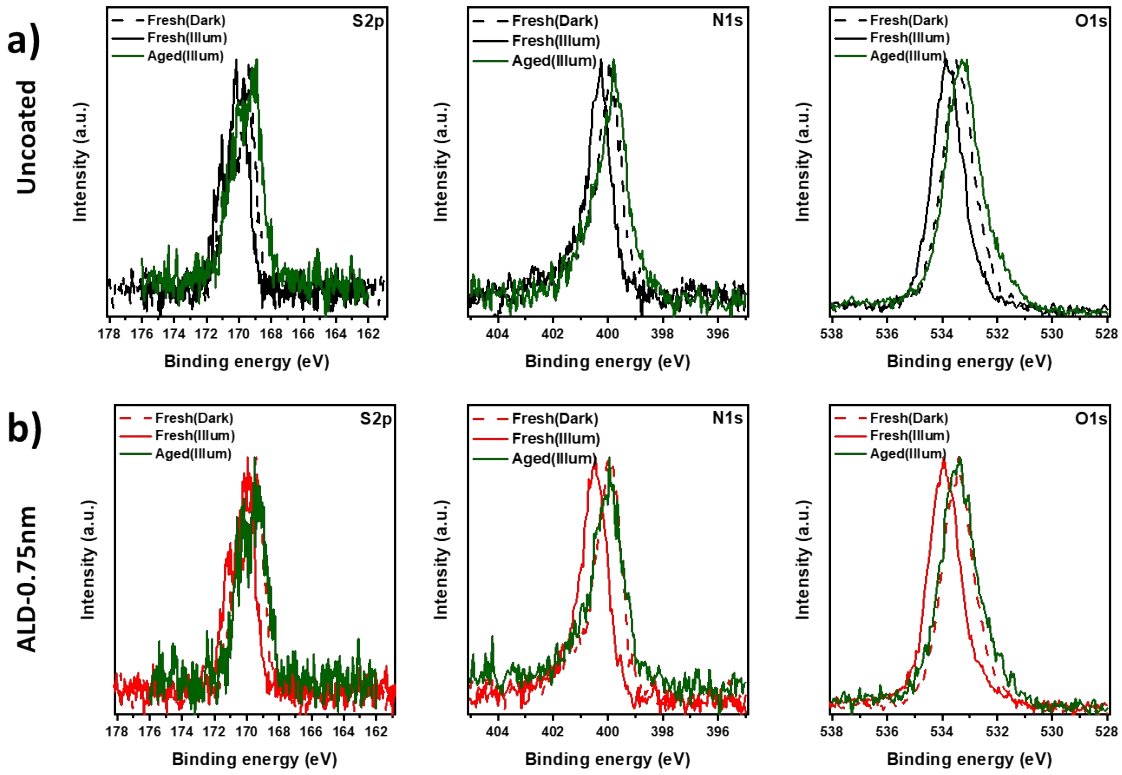

Figure S12. XPS spectra of S2p, N1s, and O1s from the spiro on a) uncoated, b) ALD-0.75nm perovskite films before (Fresh) and after in-situ aging operando aging inside NAP-XPS (Aged) during NAP-XPS under dark and illumination conditions.

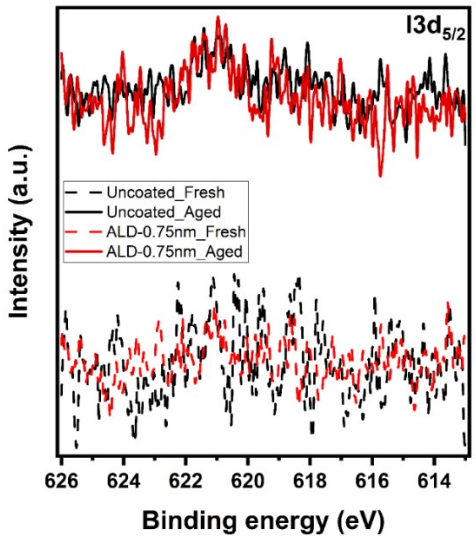

Figure S13. XPS spectra of I $3d_{5/2}$ before (Fresh) and after in-situ operando aging inside NAP-XPS (Aged) for an uncoated and an ALD-0.75 nm perovskite film.

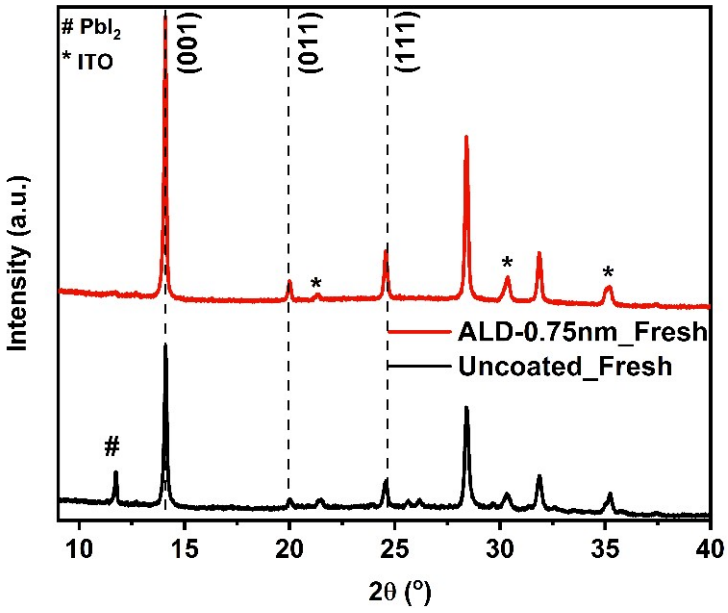

Figure S14. XRD of uncoated and ALD-0.75nm perovskite films with spiro-OMeTAD overlayer before aging (Fresh).

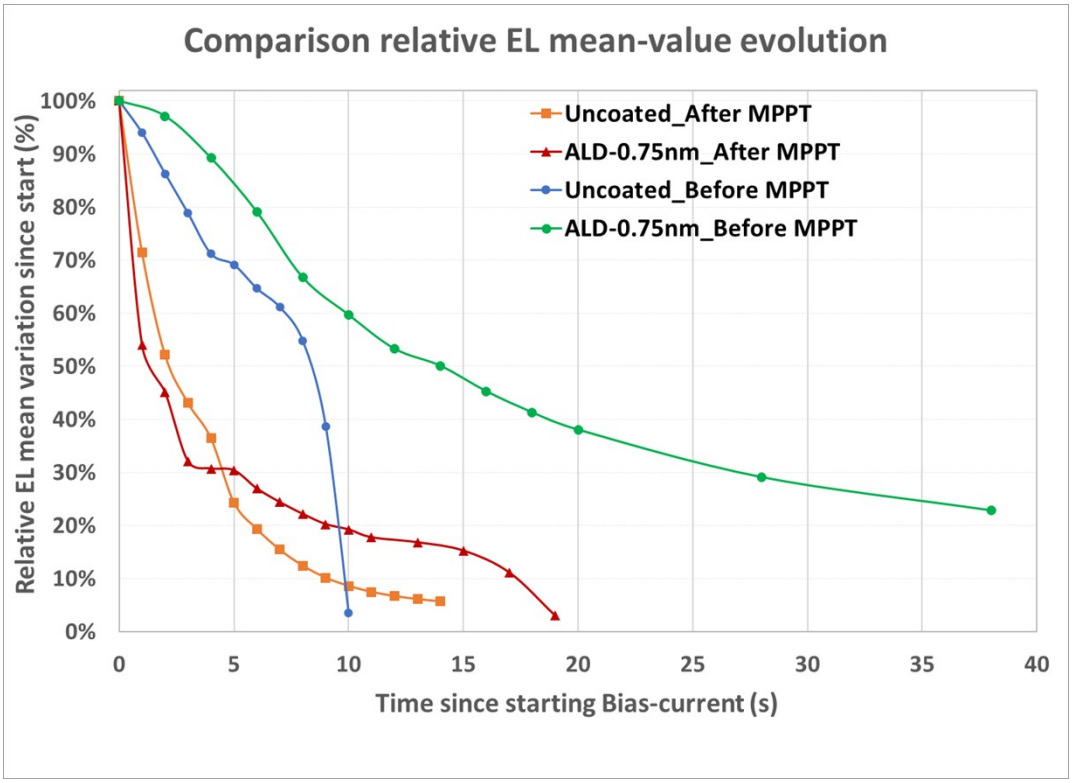

Figure S15. Mean EL time before and after MPPT for the uncoated and ALD-0.75nm devices.

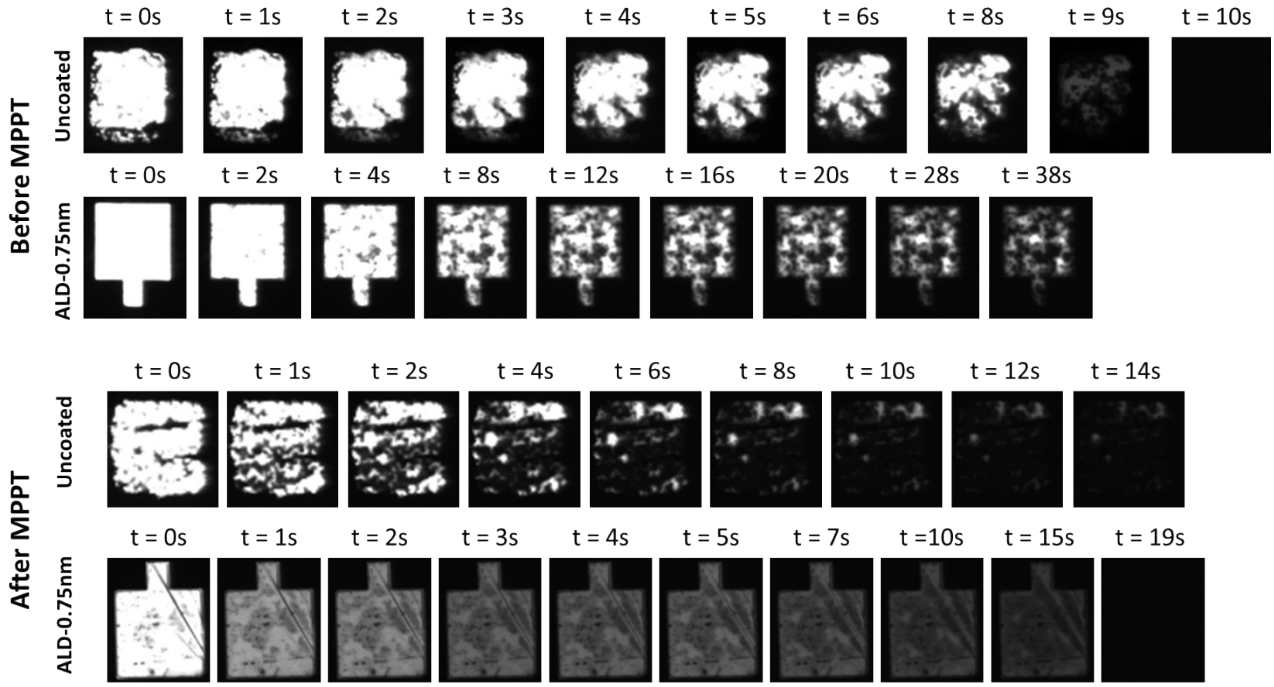

Figure S16. Series of EL images at different time intervals for the uncoated and ALD-0.75nm perovskite devices before and after MPPT. The time scale is different for each sample due to their individual lifetimes.

Figure S17. Optical images of the uncoated and ALD-0.75nm devices from the glass side illumination after the MPPT test.

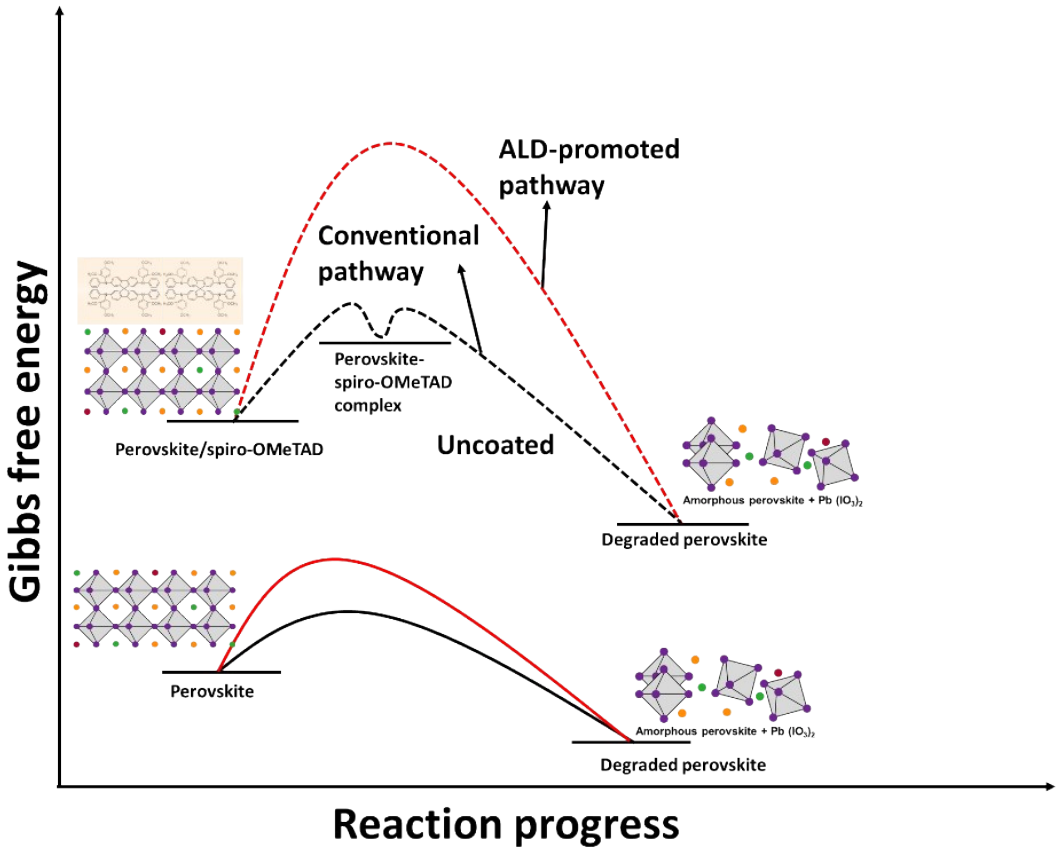

Figure S18. Gibbs free energy vs. reaction coordinate showing the degradation of perovskite with and without spiro-OMeTAD. The ALD-promoted pathway (red) has a higher activation energy vs the conventional pathway (black).

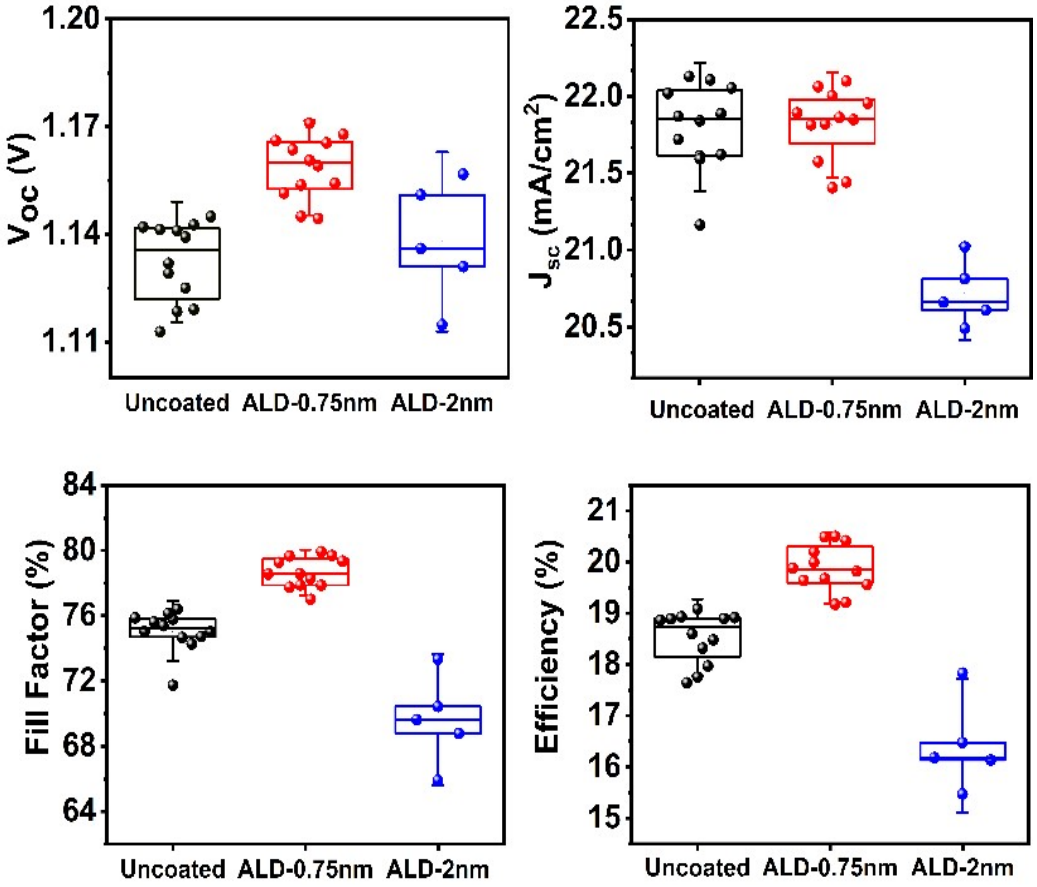

Figure S19. Statistics of photovoltaic parameters of uncoated, ALD-0.75nm and ALD-2nm devices (a) V_{OC}, (b) FF, (c) J_{SC}, and (d) PCE.

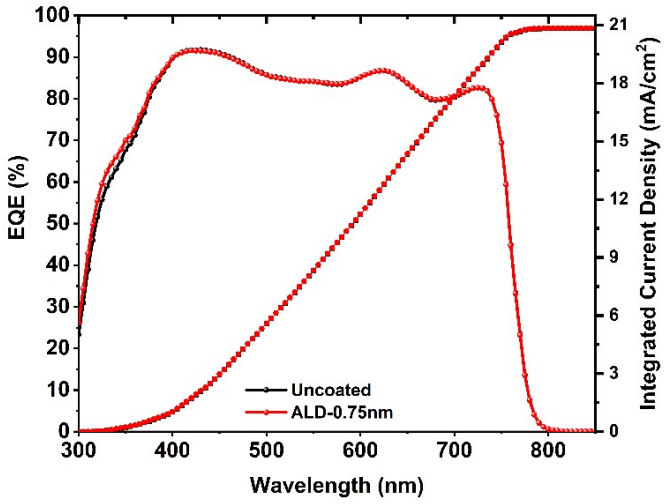

Figure S20. EQE of the of uncoated and ALD-0.75nm devices.

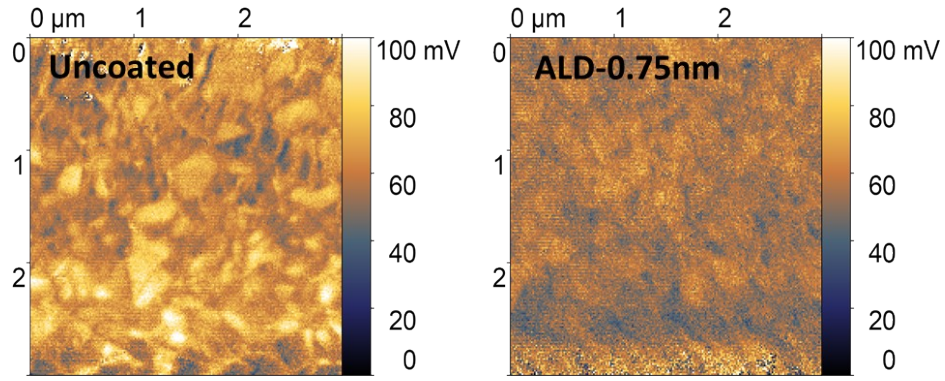

Figure S21. Surface photovoltage (SPV) of the uncoated and ALD-0.75nm perovskite films measured by KPFM.

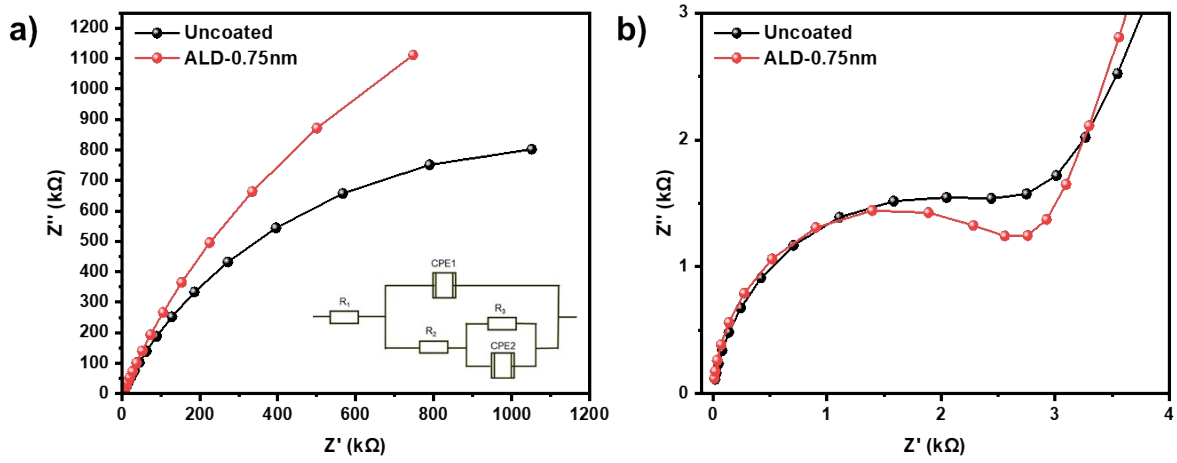

Figure S22. a) The Nyquist plots of EIS characteristics of the uncoated and ALD-0.75nm devices measured under short-circuit conditions with 10 mV AC voltage under dark in the frequency range of 0.01 Hz and 100 kHz. The inset in (a) shows the equivalent circuit. b) A zoom-in of the Nyquist plot in (a). The equivalent circuit used in the fitting of the Nyquist plot is a combination of an external series resistance (R1), two non-ideal capacitive elements called constant-phase elements (CPE1 and CPE2), and two resistive (R2 and R3) elements.

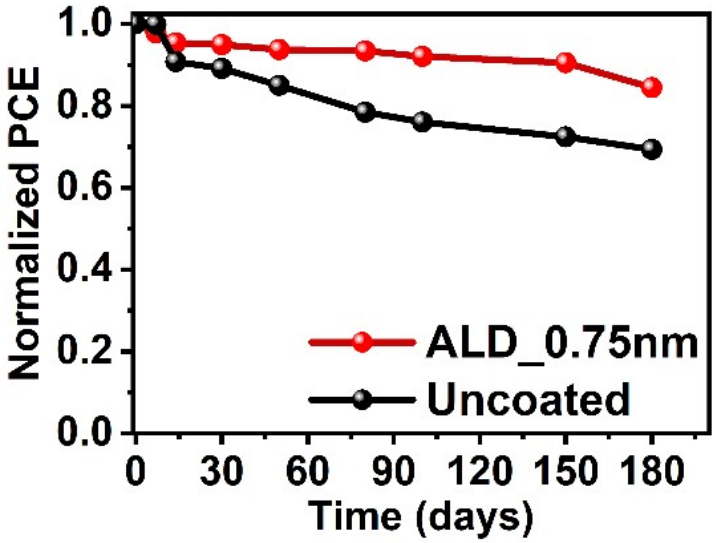

Figure S23. Normalized to 1 PCE during shelf-aging for 180 days in the dark (<10% R.H.)

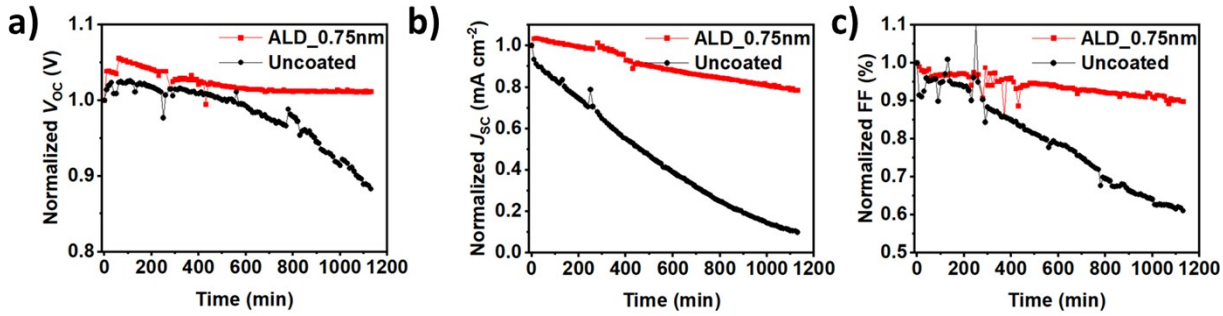

Figure S24. (a-c) Normalized to 1 Voc a), Jsc b), and FF c) as a function of time at the maximum power point (MPP). The unencapsulated 180-day shelf-aged PSCs were kept for 1000 min under ambient conditions (> 50% R.H. and 298 K) under 100 mW·cm^{-2} illumination and *J-V* measurements were performed every 10 min.

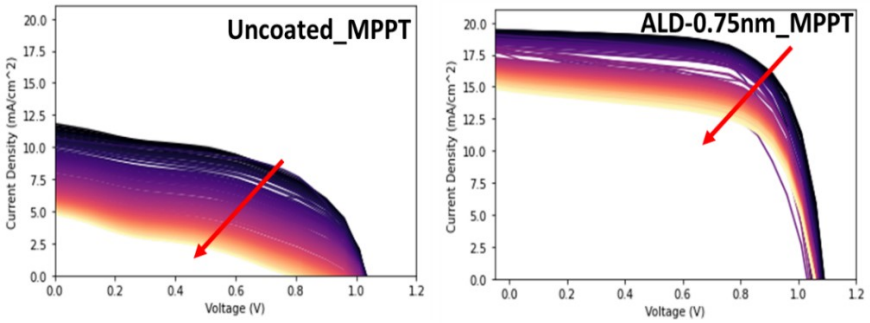

Figure S25. *J-V* curve of uncoated and ALD-0.75nm device for every 10 minutes (indicated in red arrow) during the MPPT without any encapsulation in ambient conditions.

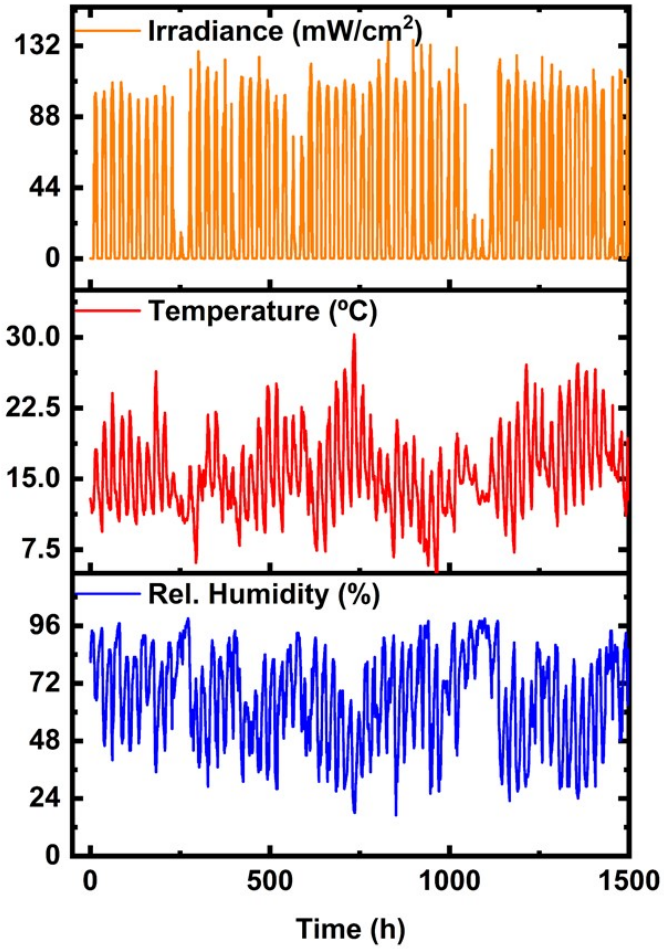

Figure S26. Corresponding irradiance, temperature, and relative humidity conditions during outdoor stability measurement in Barcelona, Spain, during the measurement period.

Table S1. Summary on main photovoltaic parameters of control and target devices.

Sample		V_{OC} (V)	J_{SC} (mA cm^{-2})	FF (%)	PCE (%)
Uncoated	Forward	1.13	21.9	76.4	18.9
	Reverse	1.14	22.0	76.2	19.1
ALD-0.75nm	Forward	1.16	22.1	79.6	20.4
	Reverse	1.16	22.1	79.9	20.5

Table S2. Fitting parameters of the Nyquist plots used for the uncoated and ALD-0.75nm perovskite devices measured by EIS.

	R_1 (Ω)	R_2 (kΩ)	R_3 (kΩ)
Uncoated	1.7	3.2	2.3
ALD-0.75nm	1.7	3.0	4.6

References:

1. Koushik D, Hazendonk L, Zardetto V, Vandalon V, Verheijen MA, Kessels WMM, et al. Chemical Analysis of the Interface between Hybrid Organic–Inorganic Perovskite and Atomic Layer Deposited Al 2 O 3. ACS Appl Mater Interfaces [Internet]. 2019 Feb 6;11(5):5526–35. Available from: https://pubs.acs.org/doi/10.1021/acsami.8b18307

2. Kot M, Das C, Wang Z, Henkel K, Rouissi Z, Wojciechowski K, et al. Room-Temperature Atomic Layer Deposition of Al 2 O 3 : Impact on Efficiency, Stability and Surface Properties in Perovskite Solar Cells. ChemSusChem [Internet]. 2016 Dec 20 [cited 2024 Feb 6];9(24):3401–6. Available from: https://chemistry-europe.onlinelibrary.wiley.com/doi/10.1002/cssc.201601186

3. Zuo W, Byranvand MM, Kodalle T, Zohdi M, Lim J, Carlsen B, et al. Coordination Chemistry as a Universal Strategy for a Controlled Perovskite Crystallization. Advanced Materials [Internet]. 2023 Sep 1 [cited 2025 Mar 20];35(39):2302889. Available from: https://onlinelibrary.wiley.com/doi/full/10.1002/adma.202302889

4. Pugliese A, Shyam B, Repa GM, Nguyen AH, Mehta A, Webb EB, et al. Atomic-Layer-Deposited Aluminum Oxide Thin Films Probed with X-ray Scattering and Compared to Molecular Dynamics and Density Functional Theory Models. ACS Omega [Internet]. 2022 Nov 15 [cited 2025 Mar 20];7(45):41033–43. Available from: https://pubs.acs.org/doi/full/10.1021/acsomega.2c04402

5. Henkel K, Kot M, Schmeißer D. Localized defect states and charge trapping in atomic layer deposited-Al2O3 films. Journal of Vacuum Science & Technology A: Vacuum, Surfaces, and Films [Internet]. 2017 Jan 1 [cited 2025 Mar 20];35(1):1–125. Available from: /avs/jva/article/35/1/01B125/246329/Localized-defect-states-and-charge-trapping-in

6. Alexander MR, Thompson GE, Zhou X, Beamson G, Fairley N. Quantification of oxide film thickness at the surface of aluminium using XPS. Surface and Interface Analysis [Internet]. 2002 Aug 1 [cited 2025 Mar 20];34(1):485–9. Available from: https://onlinelibrary.wiley.com/doi/full/10.1002/sia.1344